WET OBSERVATIONS AND SMOOTHED PARTICLE SIMULATIONS OF DQ HERCULIS

M. A. Wood[1], J. C. Simpson[2], S. D. Kawaler[3], M. S. O'Brien[3],
R. E. Nather[4], T. S. Metcalfe[4], D. E. Winget[4], M. Montgomery[4],
X. J. Jiang[5], E. M. Leibowitz[6], P. Ibbetson[6], D. O'Donoghue[7],
J. Krzesinski[8], G. Pajdosz[8], S. Zola[9,10], G. Vauclair[11], N. Dolez[11] and
M. Chevreton[12]

[1] *Department of Physics and Space Sciences and SARA Observatory, Florida Institute of Technology, 150 W. University Blvd., Melbourne, FL 32901-6988, U.S.A.*
[2] *Computer Sciences Raytheon, CSR 1310, P.O. Box 4127, Patrick Air Force Base, FL 32925-0127, U.S.A.*
[3] *Department of Physics, Iowa State University, Ames, IA 50011, U.S.A.*
[4] *Department of Astronomy and McDonald Observatory, University of Texas, Austin, TX 78712-1083, U.S.A.*
[5] *Beijing Astronomical Observatory, Chinese Academy of Sciences, Beijing 100012, China*
[6] *Department of Physics and Astronomy and Wise Observatory, Tel Aviv University, Tel Aviv 69978, Israel*
[7] *South African Astronomical Observatory, P.O. Box 9, Observatory 7935, South Africa*
[8] *Copernicus Astronomical Center, ul. Bartycka 18, 00-716 Warsaw, Poland*
[9] *Astronomical Observatory, Jagiellonian University, ul. Orla 171, 30-244 Cracow, Poland*
[10] *Mt. Suhora Observatory, Pedagogical University, ul. Podchorazych 2, 30-024 Cracow, Poland*
[11] *Université Paul Sabatier, Observatoire Midi-Pyrénées, CNRS/ UMR5572, 14 Ave. E. Belin, 31400 Toulouse, France*
[12] *Observatoire de Paris-Meudon, DAEC, 92195 Meudon, France*

Abstract. DQ Herculis was the Summer 1997 WET northern hemisphere primary target. The *O–C* phase diagram of the 71 s

signal reveals out-of-eclipse phase variations resulting from the self eclipses of a nearly edge-on, non-axisymmetric disc. We investigate the problem of simulating DQ Herculis numerically, using the method of smoothed particle hydrodynamics (SPH), and from the time-averaged structure calculate the $O-C$ phase variations as a function of inclination angle. The WET and SPH $O-C$ phase variations match to a remarkable degree, and suggest a system inclination in the range $89.5° \leq i \leq 89.7°$.

1. INTRODUCTION

For relatively recent reviews of DQ Her systems, see Patterson (1994) and Chapter 9 of Warner (1995). DQ Her was first studied as Nova 1934 Herculis, and Walker (1954, 1956) reported the then record-setting orbital period of 4^h39^m and also the bewildering 71 s signal. Warner et al. (1972) noted that this signal showed significant and repeatable phase variations during eclipse ingress and egress, but it was Bath, Evans & Pringle (1974) and Lamb (1974) who first suggested the now-accepted magnetic rotator model for DQ Her, identifying the source of the 71 s signal as the magnetic white dwarf primary's spin period, and the pulse itself as reprocessed radiation from the X-ray-emitting accretion column sweeping the inner accretion disc (see Fig 1).

Patterson, Robinson & Nather (1978, hereafter PRN) discovered out-of-eclipse phase variations near orbital phase $\phi \approx 0.7$, and suggested this was perhaps related to the expected thickening of the disc downstream of the bright spot. They also found that the pulse arrival times were color-independent, consistent with reprocessed radiation. Previous modeling attempts have tried to infer the disc rim structure and system inclination by fitting to the observed $O-C$ phase diagram of PRN (see Chester 1979, Petterson 1980, O'Donoghue 1985).

Here we work the *forward* problem of calculating the $O-C$ diagram from the disc structure given by a 3-dimensional fluid dynamics simulation, and then use these models to more tightly constrain the system parameters for DQ Her. The results presented here are a subset of those detailed in Wood et al. (2000, in preparation).
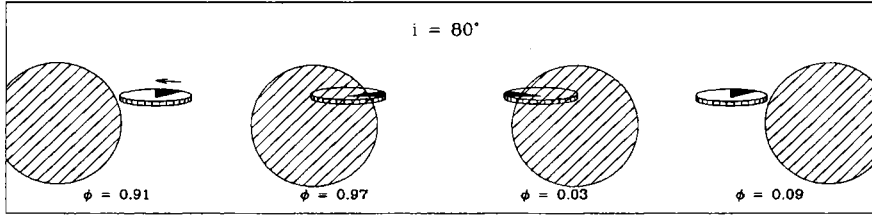
Fig. 1. A line drawing (approximately to scale) of the reprocessing region of the disc in DQ Her passing through eclipse, but viewed from an inclination angle of $i = 80°$. The EUV/X-ray beam is represented as a wedge on the disc surface, with the direction of rotation indicated by the arrow. The accreting white dwarf is located at the apex of the wedge. During ingress (egress) the reprocessed pulses will arrive earlier (later) than when out of eclipse. Note that the non-zero disc opening angle results in a front/back asymmetry in the visibility of the disc surface. For inclinations greater than $i = 90° - \langle\theta\rangle \approx 86°$, the white dwarf is permanently eclipsed by the edge-on, optically-thick accretion disc.

2. WET OBSERVATIONS

The WET campaign included both large- and small-aperture telescopes, but the results presented here include only data from the 2-m class telescopes to avoid the necessity of using a weighted average when constructing the orbit-averaged light curve. The journal of observations for these runs is given in Table 1.

The data were reduced and barycentric calculations made using standard reduction techniques (Kepler 1990). These were then converted to fractional amplitude by dividing the original data by a copy which is boxcar-smoothed with a window of 142 s in width, then subtracting unity. We use the method of Zhang et al. (1995) to obtain the orbit-averaged light curve of the 71 s signal. Specifically, we fold our fractional amplitude data on the orbital period, but shift each folded data segment by up to ± 35 s to bring it into phase with the mean 71 s ephemeris. We calculate the $O-C$ versus orbital phase diagrams of the 71 s signal by fitting a 3-cycle sine curve to the orbit-averaged lightcurve, shifting the window over the data by one cycle between fits (see Fig 4, below).

Table 1. Journal of Observations
Large Aperture Telescopes.

Run	Start Time (UTC)	Length (s)	Aperture (m)
TSM-0023	1997 Jul 1 03:32:00	24,686	2.1
TSM-0024	1997 Jul 2 03:27:30	22,434	2.1
TSM-0025	1997 Jul 3 03:19:00	26,160	2.1
TSM-0027	1997 Jul 4 06:26:00	11,720	2.1
JXJ-0007	1997 Jul 4 12:56:59	16,608	2.2
TSM-0028	1997 Jul 5 03:42:00	9,498	2.1
JXJ-0009	1997 Jul 5 14:02:10	18,088	2.2
JXJ-0010	1997 Jul 7 12:46:50	16,104	2.2
GV-0521	1997 Jul 7 22:24:00	15,878	1.9
TSM-0030	1997 Jul 8 04:35:40	13,780	2.1
JXJ-0011	1997 Jul 8 12:43:10	9,208	2.2
JXJ-0012	1997 Jul 9 15:44:10	11,036	2.2

3. SPH SIMULATIONS

We have previously used our fluid dynamics code to explore the 3-dimensional hydrodynamics of superhumps (Simpson 1995; Wood & Simpson 1995; Simpson & Wood 1998, Simpson, Wood & Burke 1998, see Monaghan 1992 for a general review of SPH techniques). Here we use the code to estimate the time-averaged equilibrium structure of the disc in DQ Her. For the runs presented here, we assume an ideal gas law $P = (\gamma - 1)\rho u$, where u is the internal energy, and we assume a "nearly-isothermal" $\gamma = 1.01$. We use the artificial viscosity prescription of Lattanzio et al. (1986)

$$\Pi_{ij} = \begin{cases} -\alpha\mu_{ij} + \beta\mu_{ij}^2 & \mathbf{v}_{ij} \cdot \mathbf{r}_{ij} \leq 0; \\ 0 & \text{otherwise;} \end{cases}$$

where

$$\mu_{ij} = \frac{h\mathbf{v}_{ij} \cdot \mathbf{r}_{ij}}{c_{s,ij}(r_{ij}^2 + \eta^2)},$$

$c_{s,ij} = \frac{1}{2}(c_{s,i} + c_{s,j})$ is the mean sound speed of the two particles, $\mathbf{v}_{ij} = \mathbf{v}_i - \mathbf{v}_j$, and $\mathbf{r}_{ij} = \mathbf{r}_i - \mathbf{r}_j$. We use $\alpha = 0.5$, $\beta = 0.5$, and $\eta = 0.1h$, where h is the particle smoothing length (effective radius).

Table 2. DQ Her system parameters.

Parameter	Value
P (h)	4.56
q	0.66
$M_1/M_\odot$	0.60±0.07
$M_2/M_\odot$	0.40±0.05
$a/R_\odot$	1.41±0.05

As we note below, we also tried $\alpha = 1.5$, $\beta = 1.0$, and the results were nearly identical with the $\alpha = \beta = 0.5$ results.

The fundamental timestep for the system is set to be $\frac{1}{1000}P_{\mathrm{orb}}$, and individual particles can have shorter timesteps if needed, in steps of factors of 2. Because all particles have the same size, an ancillary 3-dimensional mesh of spacing $2h$ and the use of linked lists allows vastly improved performance in the search/sort algorithm to identify interacting neighbor particles.

For the system parameters, we use the results of Horne, Welsh & Wade (1993) listed in Table 2.

We start with an initially-empty disc and begin by adding 2000 particles per orbit for the first 10 orbits, after which time we hold the total number of particles in the simulation at $N = 20\,000$, replacing particles accreted onto the primary or secondary or lost from the system. In about 120 orbits, the system reaches a state of dynamical equilibrium that should most closely approximate the structure of the disc in DQ Her itself, and we follow the system for an additional 100 orbits for a total of 220 orbits calculated.

Because the spatial resolution of the simulation is of order the SPH smoothing length $h \approx 0.005a$ and the particle number density is $\rho \sim 20 - 50h^{-3}$, phase-space is coarsely binned and the numerical statistical signal-to-noise ratio is low. We circumvent this problem by using the old numerical trick of averaging in time. Sampling five times per orbit insures that consecutive samples are not strongly correlated, and by concatenating the phase-space snapshots over 50 orbits in the co-rotating frame, we generate a 5 000 000-particle *ensemble disc*. We actually use consecutive 50 orbit spans from the 100 orbits calculated following the establishment of equilibrium. As expected, the two ensemble discs give effectively identical results. In addition, the solutions from higher viscosity runs with differing num-

bers of simulation particles ($N = 8000$ and $20\,000$, $\alpha = 1.5$, $\beta = 1.0$) also give essentially identical results.

We calculate the opening angle $\theta(\psi)$ of the disc as a function of the azimuth angle (in the co-rotating frame) ψ by binning the particles in the ensemble disc (minus the accretion stream) into 120 $3°$ sectors ($\sim$40 000 particles per sector). We then sort the particles in each sector by $\theta = \tan^{-1}(|z|/r)$. We make no attempt to calculate radiative transfer in our calculations, and so our disc is too hot and has no identifiable photosphere. Instead, we assume that the photospheric depth is proportional to the fractional depth in the sorted list. To give an example using round numbers, a given sector might have 10 000 particles in it, and we would calculate the "95th percentile profile" [$\equiv \theta_{95}(\psi)$] as the angle of the 9500-th particle, and the radius of the reprocessing region in this sector is taken to be the mean radius of the 200 particles with indices from 9400 to 9600.

The results of this analysis are shown in Fig 2. The top panel shows the zero-inclination view, including the positions of 20 000 particles. The outer disc is non-circular and truncated beyond $r \approx 0.4a$ (see Paczyński 1977; Osaki, Hirose & Ichikawa 1993). The bottom panel is a line drawing with several components. First, the orbital phase is labeled on a scale centered on the primary white dwarf. The secondary and white dwarf primary (innermost circle) are both shown to scale. The next circle out from the primary shows the radius that has a 71 s Keplerian orbital period, which should be the approximate Alfvén radius of the magnetic white dwarf. The solid polar histogram shows the radius of the θ_{99} profile, and the dotted one shows the θ_{95} profile in each sector – this should be roughly the radius of the reprocessing region r_{rp} as a function of ψ. Note that both profiles are circular to a good approximation and suggest $r_{\mathrm{rp}} \lesssim 0.2a$, or about one-half of the disc radius and consistent with the radius given by the eclipse-related phase shift which operates between orbital phases $\phi \approx 0.9$ and 0.1 (see, e.g., Zhang et al. 1995, their Fig. 9). The match between the radius of the reprocessing region based on the observations and that derived from the SPH calculations gives some confidence in our approach.

The next solid line is simply the outline of the disc's outer radius – specifically, the 99-th percentile radius profile.

Between the outer radius of the disk and the scale, the Figure shows the opening angle as a function of azimuthal angle as the heavy line between the reference circle just beyond the disc's radial edge and the outer scale. The radial scale is such that $r = 0$ corresponds
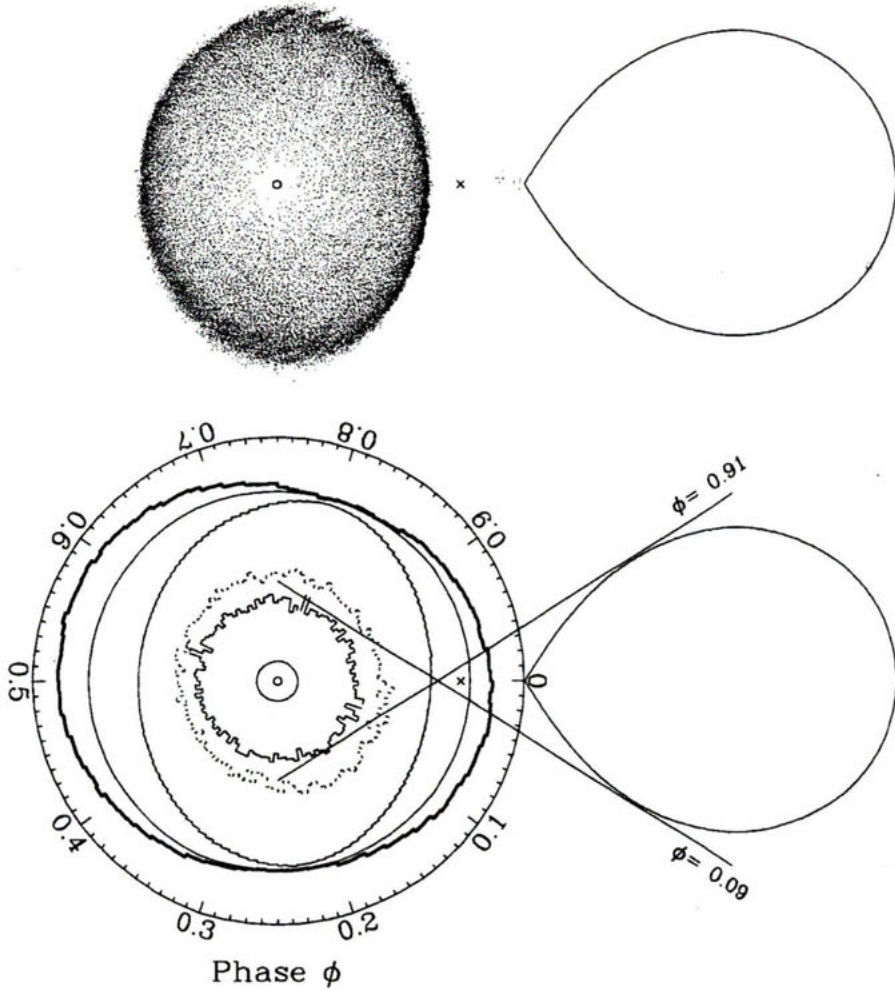
Fig. 2. The (x, y) disk projection. In the top panel, 20 000 particles are shown and the system center of mass is indicated with an "×". The bottom panel shows several features, as described in the text.

to 0°, the reference circle inside the scale corresponds to 2.73°, and the radius of the scale corresponds to 3.51°. The mean opening angle of the 95-th percentile profile is 2.94°, larger than the canonical $h/r \approx 0.015$ ($\theta \approx 1°$) suggested by the α-model, where h is the disk semi-thickness. Note however that the α-model also predicts $h \propto r^{9/8}$ which would suggest that the entire disk surface would be

able to reprocess radiation from the X-ray beam, in contrast to both observations and the hydrodynamical results here.

The opening angle of the reprocessing region is largest where the outer radius of the disk is smallest, and vice versa. If we assume a constant density fluid and roughly Keplerian velocities, then the azimuthal mass flux is proportional to the azimuthal velocity $v_\psi \propto r^{-1/2}$ times the cross-sectional area of the disk. Therefore, if the outer radius of a constant-height disk is decreased, the cross-sectional area drops proportionately, but the velocity only increases as the inverse square root. Thus to satisfy the constraint that the azimuthal mass flux is constant, the disk thickness must be largest in quadrants with the smallest radial extent. Looking back at Fig. 2, we see that indeed the surface density is highest where the outer disk radius is smallest. In large part, the rim profile of the reprocessing region is the result of the non-axisymmetric shape of the streamlines in the outer disk.
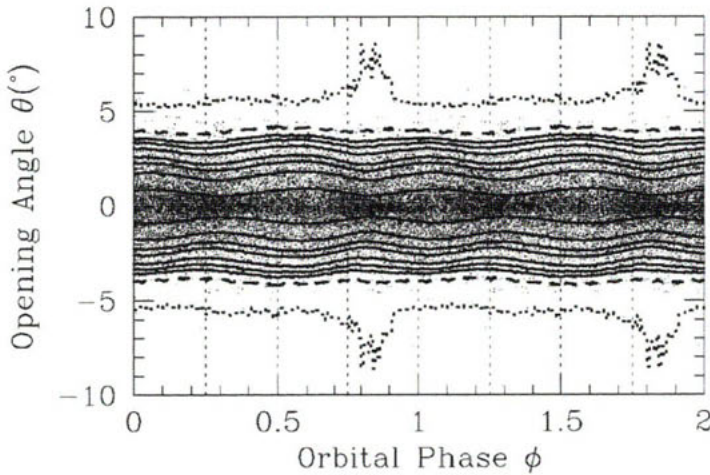

Fig. 3. The (ϕ, θ) projection of the disc. Only 30 000 particles are shown. The contour levels shown as solid lines are – moving out from the mid-plane – θ_{50}, θ_{75}, θ_{85}, θ_{90}, θ_{95}, θ_{97} and θ_{98}. The θ_{99} contour is shown as a dashed line, and the $\theta_{99.9}$ contour as a dotted line. The thickening from the accretion stream is most evident in the 99.9% contour, but only marginally evident in the 99% contour.

Fig 3 shows the θ versus ϕ projection on the disk, with the 50-th through the 99.9-th percentile contour levels plotted over 30 000

points from the ensemble disc. The contours are very similar to each other over the range θ_{75} to θ_{98}. The result of this is that the calculated $O-C$ phase variations are not a sensitive function of which profile is used over this range. It also seems likely that our profiles would not differ much if we'd included detailed radiative transfer to determine the location of the disc photosphere. Note that the accretion stream doesn't significantly affect the shape of the profile until the θ_{99} profile, and is only obvious in the $\theta_{99.9}$ profile. These profiles give $O-C$ phase variations completely unlike those observed, and so we conclude that the accretion stream must be optically thin.

We integrate over the projected reprocessing region as detailed in Wood et al. (2000, in preparation), including the light travel time across the orbit and disc. Weighting by azimuthal angle, we can calculate the $O-C$ versus orbital phase diagram as a function of inclination angle. The results for the θ_{95} profile are shown in Fig 4, where the calculated $O-C$ diagrams for inclination angles ranging from 85 to 89.9° are shown over the orbit-averaged WET $O\!-\!C$ points. The curves shown are for the 95-th percentile profile, and the best match with observations are for inclination angles between 89.5° and 89.7°. Because it is $i - \frac{1}{2}\theta$ to which these results are sensitive, if our calculated disk thickness is too large, then the inclination of DQ Her is even closer to 90°.

The total extent of the $O-C$ phase variations is less than 0.5 cycles, suggesting that we see reprocessed radiation from only one magnetic pole and that the orbital period is 71 s and not 142 s for a two-pole magnetic accretor (see Zhang et al. 1995). However, the observed points range up to 0.30 cycles at the beginning of eclipse egress, and the points appear to turn down at the end of eclipse ingress. Our current model cannot explain this observation, but we speculate that the pattern of the source of the 71 s pulsed radiation on the surface of the disk might show trailing "arms" beyond the reprocessing region itself resulting from Keplerian shear of a radial thermal pulse. Such a pattern would give rise to the observed phase behavior near totality of the reprocessing region. It may also be simply the result of a white dwarf rotation axis non-aligned with the orbital axis or perhaps reprocessing off of vertical structure beyond the calculated reprocessing region. We are currently attempting to resolve this subtle but important question.
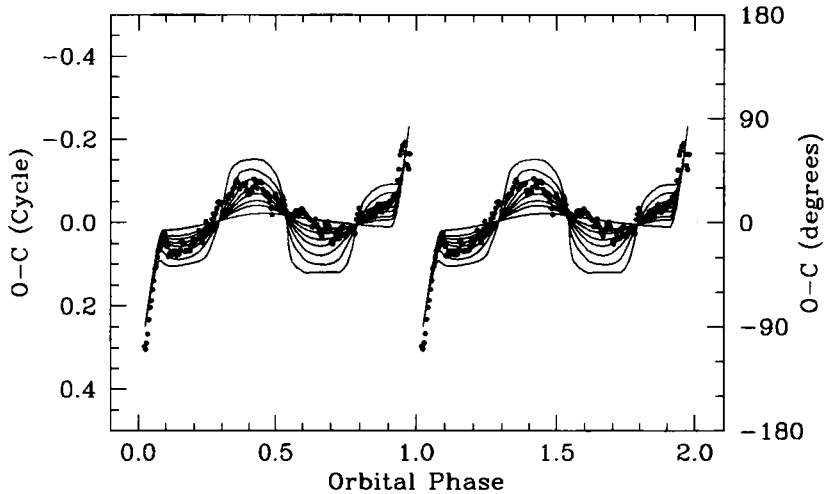
Fig. 4. The $O-C$ diagram calculated from the SPH disc structure as a function of orbital phase and for inclination angles 85°, 89°, 89.3° and 89.5° through 89.9° in steps of 0.1°. The results are very sensitive to inclination angle, and suggest $89.5° \leq i \leq 89.7$.

4. CONCLUSIONS

We can draw a number of conclusions from the above results.

- The remarkable match between the observed and calculated $O-C$ phase diagrams argues that the method of smoothed particle hydrodynamics capable of reproducing the equilibrium disc structure and statistics can be improved by averaging the results over time. Because we worked the forward problem and varied both viscosity coefficients and particle numbers in the simulations and arrived at the same match with the observational results, we can feel relatively certain that the structure we find closely approximates that in the disc of DQ Herculis itself.
- Non-circular streamlines in the outer disc are responsible for the extent and vertical structure of the reprocessing region and rim disc self-eclipse profile. The radius of the reprocessing region is only about one-half the disc radius, and results from an inflection in disk thickness vs. radius relation. While the reprocessing region is completely eclipsed, the outer disc is not, and this may in part help explain the existence of UV emission lines during mid eclipse, when the UV continuum is absent (Silber et al. 1996a,b).

These observations have also led to the suggestion that a wind is present in the system (Eracleous et al. 1998).

- The range of inclination angles which provide the best match between the observational and model result O–C phase diagrams is $89.5° \leq i \leq 89.7°$. The model results are relatively insensitive to profile chosen of the range 50-th to 98-th percentile. The accretion stream begins to appear in the 99-th percentile profile, and because it does not appear to contribute to the $O-C$ phase variations, we conclude it is optically thin.

- The O–C phase variations are sensitive to small changes ($\pm 0.1°$) in disc inclination and hence also to comparably small changes in the disc opening angle. Orbit-to-orbit as well as year-to-year variations in the $O-C$ diagram are thus naturally explained as resulting from 1–5 % changes in the disc thickness resulting, for example, from turbulent or magnetic stresses or slow changes in the mass transfer rate.

- The total amplitude of the $O-C$ phase variations is less than 0.5 cycles, and so the 71 s rotation period is favored. However, the phase variations just before and after totality of the reprocessing shows that our model is still missing some important details.

It would be useful to run an $N \approx 10^6$ simulation of DQ Her to calculate with reasonable statistics the orbit-to-orbit variations of the $O-C$ phase variations and to compare these with those present in the WET observations. It would also be interesting to use the velocity and relative temperature fields of the "ray-traced surface particles" (see Simpson, Wood & Burke 1998) as a basis for calculating the spectrum as a function of orbital phase. Both projects should provide even tighter constraints on fundamental system parameters for DQ Herculis.

REFERENCES

Bath G. T., Evans W. D., Pringle J. E. 1974, MNRAS, 166, 113

Chester T. J. 1979, ApJ, 230, 167

Eracleous M., Livio M., Williams R. E., Horne K., Patterson J., Martell P., Korista K. T. 1998, in *Wild Stars in the Old West*, eds. S. Howell, E. Kuulkers & C. Woodward, ASP Conf. Series, 137, 438

Horne K., Welsh W. F., Wade R.A. 1993, ApJ, 410, 357 (HWW)

Kepler S. O. 1990, in *The Second WET Workshop Proceedings*, eds. E. Meištas & J.-E. Solheim, Baltic Astronomy, 2, 515

Lamb D. Q. 1974, ApJ, 192, L129

Lattanzio J. C., Monaghan J. J., Pongracic H., Schwarz M. P. 1986, J. Sci. Stat. Comput., 7, 591

Monaghan J. J. 1992, ARA&A, 30, 543

O'Donoghue D. 1985, in *Proc. 9th North Am. Workshop on Cataclysmic Variable Stars*, ed. P. Szkody, Univ. of Washington, Seattle, p. 98

Osaki Y., Hirose M., Ichikawa S. 1993 in *Accretion Disks in Compact Stellar Systems*, ed. J. C. Wheeler, World Science Publ., Singapore, p. 272

Paczyński B. 1977, ApJ, 206, 822

Patterson J., Robinson E. R., Nather R. E. 1978, ApJ, 224, 570

Patterson J. 1994, PASP, 106, 209

Petterson J. 1980 ApJ, 241, 247

Silber A. D., Anderson S. F., Margon B., Downes R. A. 1996a, ApJ, 462, 428

Silber A. D., Anderson S. F., Margon B., Downes R.A. 1996b, AJ, 112, 1174

Simpson J. C. 1995, ApJ, 448, 822

Simpson J. C., Wood M. A. 1998, ApJ, 506, 360

Simpson J. C., Wood M. A., Burke C. J. 1998, in *The Fourth WET Workshop Proceedings*, eds. E. G. Meištas & P. Moskalik, Baltic Astronomy, 7, 255

Walker M. F. 1954, PASP, 66, 230

Walker M. F. 1956, ApJ, 123, 68

Warner B. 1995, *Cataclysmic Variable Stars*, Cambridge

Warner B., Peters W. L., Hubbard W. B., Nather R. E. 1972, MNRAS, 159, 321

Wood M. A., Simpson J. C. 1995, in *The Third WET Workshop Proceedings* eds. E. G. Meištas & J.-E. Solheim, Baltic Astronomy, 4, 402

Zhang E., Robinson E. R., Stiening R. F., Horne K. 1995, ApJ, 454, 447